Effect of the addition of Si into V_2O_5 coatings: Structure and tribo-mechanical properties

Roberto Mirabal-Rojas[1,2], Sandra E. Rodil[1], Giovanni Ramirez[3,4], Tomas Polcar[5], Enrique Camps[6], Ali Erdemir[3]

[1] Instituto de Investigaciones en Materiales, Universidad Nacional Autonoma de Mexico, Circuito Exterior s/n CU, CDMX. 04510, Mexico.

[2] Current address: Becton Dickinson de México S.A. de C.V., Calle Monte Pelvoux 111 Piso 8 Depto. PH, Lomas de Chapultepec, Miguel Hidalgo, CDMX. 110000. México

[3] Energy Systems Division, 9700 S. Cass Ave, Argonne National Laboratory, Argonne, IL, 60439

[4] Current address: Bruker Nano Surfaces, 61 Daggett Dr, San Jose, CA, 95134

[5] nCATS, University of Southampton, Highfield, SO17 1BJ Southampton, UK

[6] Instituto de Nacional de Investigaciones Nucleares, Carretera México-Toluca S/N, kilómetro 36.5. La Marquesa, Municipio de Ocoyoacac. CP 52750, Estado de México, Mexico.

*Corresponding author e-mail: srodil@unam.mx;

Abstract

Vanadium oxide (V_2O_5) is one of the lubricious oxides with the potential to be used as a solid lubricant at elevated temperatures. However, the material itself is not hard wear-resistant, so most of the research has focused on adding V into hard nitride coatings that could lead to the formation of a self-lubricating V_2O_5 layer when heated. The other possible solution, which has been less studied, is to look for mechanisms to enhance the hardness of the oxide coating. In this research, we investigate the effect of the addition of Si into the V_2O_5 coatings, aiming to find conditions that lead to enhance hardness and/or reduced wear while keeping the high

temperature lubricity of the V_2O_5 structure. For this, Si modified V_2O_5 coatings were deposited using a dual magnetron sputtering system. The results showed that small additions of Si (< 2.0 at%) improved the hardness of the V_2O_5 coatings up to 5 times while keeping the same temperature dependence of the coefficient of friction than V_2O_5. Dry sliding experiments using the pin-on-disc configuration against silicon nitride balls were performed at 25, 300 and 600 °C. Wear factors in the 10^{-7} mm^3/Nm range were obtained, indicating a good wear resistance. Further addition of Si into the V_2O_5 structure led to a loss of the crystalline ordering and a significant reduction in the hardness.

Keywords: Sputtering; Tribological coatings; Hall-Petch; Hardening; Oxidation resistance; Lubricity.

1 Introduction

The development of solid lubricants for contacts under mixed or boundary lubrication conditions, as well as for open air, high humidity and high temperatures (above 500°C), is of special interest for the automotive and aerospace industries. Under these environmental conditions, most of the sliding surfaces will oxidize, therefore the oxide films will dominate the friction and wear behavior of the interfaces. The recent research has shown that certain oxides, known as lubricious oxides [1-5], have low shear strength at elevated temperatures and hence could be used as solid lubricants. These oxides could provide significant oxidation resistance and fairly low friction at elevated temperatures. However, the lubricious oxide coatings are not considered as protective coatings for mechanical applications, since they are mechanically soft. Therefore, most of the research has focused on the addition of elements of the forming oxides into hard metal nitride coatings, aiming to obtain the high temperature low friction, but keeping the hardness of the metal nitride matrix [6-8]. Franz et al. [9] presented a review paper about the use of VN coatings or V-containing nitride hard coatings

as solid state lubricants. Meanwhile, V into ZrO_2 coatings has also been shown to produce low friction at high temperatures [7].

Vanadium oxide is one of the most studied lubricious oxides, particularly the orthorhombic α-V_2O_5, which is the stable crystalline structure. It clearly shows a decrease in the coefficient of friction (CoF) as the working temperature is increased, which has been explained in terms of its layered structure. The α-V_2O_5 is built up from VO_5 square pyramids shearing edges and corners. Thanks to the weak V-O interactions (van der Waals type) which held the V_2O_5 layers, this phase and the Magnelí phases [10, 11] are promising solid lubricants, as described in details by several researchers [4, 12-16].

Fateh et al. [17, 18] and Lugscheider et al. [19] have evaluated the mechanical and tribological properties of V_2O_5 coatings deposited by the magnetron sputtering (MS) technique. Fateh et al. [17] reported that the transition from amorphous to polycrystalline growth with increasing deposition temperatures yields an increase in hardness and Young's modulus; the hardness of the crystalline V_2O_5 coatings varied between 3-7 GPa. In another study [18], they deposited V_2O_5 coatings by reactive magnetron sputtering on high speed steel and their tribological behavior under different temperatures was investigated. Ball-on-disc experiments against alumina showed that the CoF of all investigated coatings decreases with increasing temperature and cause an improvement in the wear resistance. The CoF decreases from 0.55 at RT to 0.39 at 300 °C and reaches its lowest value of 0.15 at 600 °C. These values were similar to those obtained by Gulbinsky et al. [20] who used pulsed dc magnetron sputtering to deposit V_2O_5 onto alumina substrates. Conversely, Lugscheider et al. [21] used MS ion platting and found that the V_2O_5 phase could be produced for substrate temperatures above 350 °C. No high temperature friction measurements were done, but the room temperature characterization and thermal stability of the coatings suggested that the coatings were promising for self-lubricating applications at elevated temperatures.

However, no works have attempted to enhance the mechanical properties of low CoF oxide coatings, using some of the already known hardening strategies such as nanostructuring or solid solution hardening [22-26].

The objective of the present work is to explore the effect of Si additions into the structure, and the mechanical-tribological properties of crystalline magnetron sputtered V_2O_5 coatings aiming to increase the hardness and/or reduce wear while keeping the low CoF at high temperatures. The effect of Si addition on the structure and hardness of oxide coatings has not been deeply explored. Voevodin et al. [27] obtained $AlSiO_x$ coatings by electrochemical oxidation of Al alloys using a high voltage spark treatment in an electrolyte bath containing $NaSiO_3$, resulting in the incorporation of SiOx into the Al_2O_3 coating. The results showed the synthesis of a composite coating consisting of hard Al_2O_3 phase (18-25 GPa) in a soft matrix of alumina-silicate phase (2 GPa). The application of this coating decreased the wear rate of components fabricated from an Al-based alloy by several orders of magnitude and permitted operation of coated friction pairs at 1 GPa contact load. In a previous paper [28], we have reported the effect of Si addition into niobium oxide coatings deposited by co-sputtering. The results showed that the addition of Si lead to a reduction in the grain size and an increase in the hardness from 8.4 to 17.6 GPa. However, it was not possible to obtain a uniform Nb_2O_5 phase and the samples were constituted of 20-30% of an amorphous substoichiometric niobium oxide. For those $NbSiO_x$ samples, high temperature tribological evaluation was not performed. The effect of the addition of Si into the tribological properties of CrN or CrAlN was investigated by Park et al. [29], showing that the addition of about 9 at% of Si lead to significant increments in the hardness and a reduction in the room temperature CoF. Such modifications were driven by the formation of a composite architecture consisting of nanosized (Cr,Si)N or (Cr,Al,Si)N crystallites embedded in an amorphous Si_3N_4/SiO_2 matrix. More recently, Lu et al. [30] added Si into CrMoN coatings and evaluate the high

temperature CoF of the coatings. The results showed that the CoF of Cr-Mo-Si-N increased with Si addition, effect that was attributed to less amount of lubricant oxide (MoO_3) and more SiO_2. However, no additional works about the addition of Si into oxide coatings and particularly into V_2O_5 were found.

2 Experimental Procedure

2.1 Deposition Conditions

Since the V-O system includes VO, VO_2, V_2O_3 and V_2O_5 and non-stoichiometric phases, preliminary experiments were done to obtain coatings with a predominant α-V_2O_5. It was found that α-V_2O_5 was obtained under an oxygen flow rate of 8 sccm (standard centimeter cubic meters), argon flow rate of 24 sccm and total chamber pressure of 0.25 Pa. Pure vanadium (99.95% purity) and silicon (99.999% purity) targets were used to deposit the V_2O_5:Si coatings on polished D2 steel disks. A confocal magnetron sputtering system was used in which the magnetrons (10 cm diameter) were positioned with an angle of 53° to the vertical axis and substrate-target distance of 100 mm. The substrates were mounted on a rotary sample holder (15 rpm) and heated up to 350 °C during the deposition process. In order to obtain V_2O_5:Si coatings with different Si contents, the direct current (DC) power applied to the V target was fixed at 400 W, while different radio frequency (RF) powers were applied to the Si target (12-200W). The deposited coatings were named according to the *power applied to the Si target* (PASi), namely V_2O_5-PASi (PASi= 0, 12.5, 25, 50, 75, 100, 150 and 200W). A 100 nm V buffer layer was grown on the D2 substrates using only Ar and the V target for 10 min. Then, O_2 was added to the gas phase and the power applied to the Si target was set-on. After this, both magnetrons were operated at the same time using the Ar/O_2 mixture. The deposition time was fixed to 240 min (plus the 10 min of the V bonding layer) in order to determine the effect of the power applied to the Si target on the deposition rate.

2.2 Coatings Characterization

The surface morphology and the composition of the coatings were obtained using a JEOL7600F field emission-scanning electron microscope (FE-SEM) with 10 kV of acceleration voltage. The composition and chemical structure was measured using X-ray photoelectron spectroscopy (XPS). The XPS spectra were obtained in a Versa-Probe II Physical Electronics system using the Al-Kα line after mild Ar cleaning of the surface (0.5kV, 500 nA). The binding energy was referred to the C1s spurious signal at 284.5 eV. The thickness of the coatings was evaluated using a Veeco Dektak 150 profilometer measuring the height of a step left in a small-uncoated area. The structural characterization was done using a Rigaku Ultima IV diffractometer (CuKα 1.5406 Å) in the grazing incidence (at 1°) mode to avoid the fluorescence from the steel substrate. Micro-Raman Spectroscopy was done using a Horiba T64000 with an INNOVA 70C spectrum laser with a wavelength of 514 nm.

Mechanical properties (hardness and elastic modulus) were evaluated by nanoindentation using a CSM Instrument model TTX with a Berkovich-type pyramidal diamond tip. The applied loads were between 1 and 3 mN, taking care that the penetration depth did not exceed 10% of the coatings thickness [31]. The reported hardness and elastic modulus are the average of six different measurements and calculated using the Oliver-Pharr model [32]. Dry sliding experiments (by triplicate) were conducted using the coated D2 steel discs in ambient air at 25 °C, 300 °C and 600 °C, using a CSM THT high-temperature pin-on-disc tribometer and Si_3N_4 balls of 6 mm diameter as counterpart. For all the coatings, the applied load was 1N; sliding speed was kept constant at 0.1 m/s, while the sliding distance was 50 m. After tribometer testing, the wear tracks on the coatings were characterized; collecting 5 scans on each track using the DEKTAK profilometer, and the wear volume was estimated using the

standard wear-rate equation. Wear tracks of the samples were examined using Raman spectroscopy (Horiba Jobin-Yvon LabRAM Raman Microscope, He–Ne laser, k = 632.8 nm)

3 Results

3.1 Morphology and Composition

Figure 1 (a-h) shows the surface morphology of all deposited coatings. The contrast of the backscattering images indicated bright agglomerates with similar composition (V_2O_5) surrounded by intergranular dark spaces, probably composed of low atomic mass elements such as air and the SiO_x phases. However, at this scale, energy dispersive fluorescence maps were not able to detect Si-segregated phases. A noticeable change in the surface morphology can be observed by increasing the PASi. The first samples (V_2O_5-0 to V_2O_5-50) showed large grains composed of agglomerated bars with clear crystalline facets, but changed into slanted plates for the V_2O_5-75 sample and then to a more disorder structure for the last three samples (V_2O_5-100 to V_2O_5-200), where the crystalline facets were not clearly distinguished. The bar-like morphologies are similar to those presented by Fateh [18] for the V_2O_5 single layer coatings after heating during the tribological tests, and also to the crystalline V_2O_5 coatings produced by Lugscheider et al.[19] and the pulsed laser deposited V_2O_5 samples at 500 °C [33]. Table I shows the variation of the thickness as a function of the PASi for the samples deposited on the D2 steel. It can be observed that the film thickness rises linearly from 1245 ± 49 nm to 2298 ± 46 nm as the PASi increases, which is a consequence of both the incorporation of Si into the coating, but also that the secondary power enhances the plasma density and so the sputter rate.

The composition was obtained from analysis of the XPS data using the Multipak® database. Examples of the survey spectra and the high-resolution V 2p and O 1s regions can be observed in Figures S1 and S2, where it can be observed that the Si addition into the samples

modifies the chemical environment of oxygen due to the formation of Si-O bonds, while the V bonding state remained unaltered. Figure 2(a) shows the high resolution Si 2p photoelectron signal that is centered on 103 eV indicating that Si is primarily bonded to oxygen, forming Si-O bonds. The Si content and V/O ratio measured by XPS can be seen in Figure 2 (b). For PASi values lower than 50W, no signal from Si was obtained in the XPS spectra. Initially, the rate of Si incorporation is very slow, but the Si content rises significantly to 7.1 ± 0.1 at% at 100 W and reaches a maximum value of 9.7 ± 0.1 at% for the sample deposited at 200 W. The V/O ratio remained nearly constant (close to the stoichiometric 0.4 value) for PASi between 0 and 100, and beyond this power, it decreases. Such decrement is associated to the higher Si incorporation and the competence between V and Si for the oxygen, whose flow rate was kept fixed. The enthalpy of formation of Si-O bonds (-911 kJ/mol) is much lower than that of V-O bonds (-1557 kJ/mol), so under reactive growth conditions, it is expected that Si will bond easier to O leading to formation of SiO_x phases [34] and depleting the vanadate phase from oxygen.

3.2 Structure by XRD

The XRD patterns of the V_2O_5:Si coatings deposited under the different deposition conditions are presented in Figure 3, the patterns were normalized between 0 and 1, using their corresponding maximum signal. The predominant detected phase is orthorhombic α-V_2O_5 (ICDD-00-041-1426) with variations in the preferred orientation, peak width and intensities (Figure S3). The first four coatings (V_2O_5-0 to V_2O_5-50) showed a mixed orientation along the (200) and (001) planes, a finding which has not commonly been obtained in previous works reporting the growth of V_2O_5 coatings by sputtering [20, 35-37]. However, as the power applied to the Si target increased, there was a change in the preferred orientation; the (001) is the predominant orientation for both V_2O_5-75 and V_2O_5-100 samples. Nevertheless, the total intensity of the diffraction peaks was larger for the V_2O_5-75 sample than the V_2O_5-

100 sample, suggesting that the 100 W deposited sample had lower long-range ordering. For the V_2O_5-150 sample the (001) orientation persisted but there was a new diffraction peak place at 25° that could be attributed to the V_2O_5 phase or to the formation of strained SiO_2; these diffraction peaks were less intense and broader indicating the formation of even smaller nano-crystallites. Finally, for the PASi 200 W, only the weak and very broad peak centered around 25° was observed.

The modifications in the preferred orientation of the coatings agree with the differences in the surface morphology (Figure 1). The first four samples deposited with the lowest PASi present the same type of morphology of agglomerated bars in good agreement with the similar XRD patterns. The V_2O_5-75W shows a completely different morphology composed of very well crystallized slanted plates, as well as the larger diffraction peak intensities (Figure S3). As the PASi (≥ 100 W), the morphology looks more disordered without clear faceted crystals, which is also reflected in the reduced diffraction intensity and peak broadening suggesting that the films are composed of a mixture of fine crystallites and amorphous phase.

The incorporation of Si into the V_2O_5:Si coatings structure induced a progressive reduction of the crystalline domains from 38 ± 2 nm (V_2O_5 coating) to 6 ± 2 nm for the V_2O_5-150 sample, which was estimated applying the Scherrer relationship to the main diffraction peak (Table I).

3.3 Raman spectroscopy

Figure 4 shows the micro-Raman spectra of the coatings. The Raman spectra present the characteristic bands of the α-V_2O_5 phase [38, 39]. There is a very good correlation between the XRD and Raman spectra. In both cases, there is a larger total intensity for the samples deposited using PASi between 50 - 75 W, and for further power, the intensity decreases rapidly. The Raman spectra, however, are not sensitive to preferred orientation, so they remain very similar up to 150 W, where broadening and the appearance of new peaks

between 800-1100 cm^{-1} were observed. However, none of these peaks are related to Si-based Raman bands, which help to rule out the assignment of the $2\theta = 25°$ diffraction peak to SiO_2.

More detailed information about the degree of order in the V_2O_5 structure can be obtained by analyzing peaks related to internal and external modes. The external or lattice vibrational bonds are at low frequencies (< 200 cm^{-1}) while all the other peaks are related to internal modes related to the different V-O environments and symmetries [14, 40]. The intense peak around 144-148 cm^{-1} and two smaller peaks, 101-107 cm^{-1} (not seen in our spectra) and 195-201 cm^{-1}, are characteristic of the layered (sheet-like) structure of the V_2O_5 structure, so they are indicative of the formation and ordering of the V_2O_5 phase. By fitting the 144 cm^{-1} peak using a Lorentzian peak, a small shift to higher wavenumbers as a function of the Si content was observed (from 144.34 for V_2O_5-0 to 147.3 cm^{-1} for V_2O_5-150). Since this vibration band is related to the weakly bonded sheets, the shift into high wavenumbers indicates that the inter-sheet distance has decreased. The peak width remained between 7.7-8.9 cm^{-1}, without a clear trend, for all samples except for V_2O_5-150 and V_2O_5-200. In those samples, the peak width increased up to 11 cm^{-1}, suggesting a larger degree of disorder in them.

This disorder is also confirmed by the appearance on these two samples of three internal modes at 848, 882 and 940 cm^{-1}, which are not associated to Raman active modes of the V_2O_5 structure. It is likely that these three bands are IR active bands that became Raman active due to disorder. Abello et al. [40] have reported the IR spectra and theoretical calculations of the IR spectra of orthorhombic V_2O_5, finding in all cases three vibrational modes around 821, 985 and 1017 cm^{-1}. The difference in the wavenumbers might be associated to oxygen deficiencies or the disorder induced by the addition of Si into the V_2O_5 coatings. According to Julien et al. [12] and Ramana et al. [14] the 848 cm^{-1} band is Raman inactive for a crystalline V_2O_5 structure, but it is active due to loss of crystalline ordering, so

it is called a disorder mode. The 940 cm^{-1} peak was also observed by Lee et al. [41] at 932 cm^{-1} and was associated to the stretching vibration of V^{4+}=O bonds, which became more evident in oxygen-deficient samples.

The most characteristic internal mode of the V_2O_5 structure is the stretching mode at 996 cm^{-1}, which is related to the vanadyl group (V=O), where O is a terminal atom [40]. Analysis of this peak is interesting, since shifts of this peak to lower wavenumbers are indicative of the weakness of the V=O bonding and observed in oxygen deficient V_2O_5. In our samples, the peak was fitted using a Lorentzian and the peak position increased only slightly from 996.6 to 997.8 cm^{-1} with the Si content. This shift was therefore not indicative of oxygen deficiencies, suggesting that the three bands observed should be related to the disorder.

The structural characterization (XRD and Raman) indicated that the SiO_x signal detected from the XPS must be associated to an amorphous SiO_x component, which might be distributed forming a thin layer surrounding the V_2O_5 crystallites. However, high resolution transmission electron microscopy might be necessary to confirm this assumption.

3.4 Nanoindentation

The hardness and Young's modulus were obtained using the nanoindentation method, which provides information on the mechanical properties of the materials through modeling of the indenter load-displacement curves. In this study, indentation loads were used in such a way that the penetration depth was less than 10% of the coating thickness in order to obtain the coating-only hardness. Figure 5 shows the hardness and elastic modulus of the V_2O_5-PASi coatings deposited on the D2 substrate as a function of the PASi. It can be seen that the hardness value obtained for the V_2O_5-0 sample is 3.6 ± 0.25 GPa, which is similar to that reported by Fateh et al. [42] for α-V_2O_5. By increasing the Si content, the hardness increased

to 16.1 ± 0.2 GPa for the V_2O_5-75 sample, nearly five times more than V_2O_5 coating. However, further increment in the Si contents led to a decrease in hardness values, down to 2.9 ± 0.2 GPa for the V_2O_5-200 sample. The elastic modulus, also shown in Figure 5, presented a similar trend to that of the hardness. The values increased from 132.4 ± 3.5 GPa for the V_2O_5-0 to 240.9 ± 3.5 GPa for the V_2O_5-75 and finally decreased to 127.4 ± 2.5 GPa for the V_2O_5-200.

Figure 5 shows that the variations in the mechanical response of the coatings are mainly due to the structural changes induced when the power applied to the Si target was increased, more than to the Si content itself. It is well known that hardness and elastic modulus of polycrystalline metals and ceramics can be improved through the grain size refinement or the Hall-Petch effect [43-46], where the relationship between the hardness and the grain size is given by the following equation:

$$H = H_0 + k_h d^{-1/2} \quad (1)$$

Where H is the hardness of the material, d is the grain size and the H_o and k_h are constants related to the material [43-46].

Figure 6 shows the graphical representation of equation (1), hardness versus the square root of the inverse of the grain size. For V_2O_5-PASi (< 75W) coatings, where the hardness enhancement was observed, a relative good linear fit can be obtained (R^2=0.94). This linear fit suggests that the hardening mechanism of the V_2O_5 coatings can be explained as a consequence of the refinement of the crystalline structure as the power applied to the Si target was increased. The grain size reduction might have been caused by the segregation of Si into the grain boundaries, forming an amorphous SiO_x phase. For the samples deposited at low PASi (12.5 and 25 W), the Si incorporation could not be confirmed, but the reduction in the

domain size and hardening effect observed (Fig. 5 and Fig. 6) suggest that the Si amount was below the detection limit of the equipment. Beyond 75W, the crystalline domain size was further reduced and nevertheless, the hardening effect was completely lost. This could be explained in terms of the anomalous or reversed Hall-Petch effect, which predicts a minimum domain size; beyond this value a different deformation mechanism is established (grain boundary sliding instead of dislocation related deformation), which would explain the lower hardness [45-48]. Moreover, for the samples with larger Si incorporation (PASi ≥ 100 W), other effects could also contribute to the decrease in the hardness, such as the reduction in the long-range order of the crystalline structure and the larger fraction of the segregated-amorphous SiO_x layer.

A summary of the coating characterization data is presented in Table I, which includes the PASi value, thickness, the Si at%, the V/O composition ratio, crystalline domain size and the nanoindentation results.

3.5 Tribological characterization

The tribological characteristics (CoF and wear rate) of the coatings were obtained by the pin-on-disk measurements at three different temperatures (25, 300 and 600 °C). The tribological characterization is reported only for the samples that retained the V_2O_5 crystalline structure, i.e. for PASi between 0 and 75. Figure 7 illustrates the CoF of the coatings as a function of the homologous temperature, T/T_m, where T_m is the melting point of the V_2O_5 (T_m= 610 °C). The expected decrease in the CoF of the V_2O_5 for high T/T_m values is clearly observed for all samples, indicating that Si addition and the structural changes did not affect this fundamental property. However, the CoF of the samples with larger Si content (samples V_2O_5-50 and V_2O_5-75) was slightly larger at the highest temperature, which might be related to the tribological properties of the SiO_x phase.

The dimensions of the wear scars (depth and wideness) were measured using profilometry for all samples and conditions. It was found that penetration of the ball into the coatings in its maximum value reached 94% of the coating thickness. The wear rate as a function of power applied to the Si target for the three measurement temperatures is plotted in Figure 8a. It can be observed that the wear rate of the coatings deposited at PASi ≤ 50 is not significantly different, although a small decrease in the wear rate is observed as a function of the homologous temperature. On the other hand, the V_2O_5-75 sample presented a significantly lower wear rate for RT and 300 °C, but at 600 °C, all films presented similar values about 2-3 × 10^{-7} mm^3/Nm. These wear rates were in the 10^{-7} mm^3/Nm range can be considered as a good wear resistance for coatings [49]. The enhanced wear resistance presented for the V_2O_5-75 sample at lower homologous temperature is probably related to the well-ordered and (001) textured crystalline structure obtained for this sample. Figures 8b and 8c show representative Raman spectra measured inside and outside of the race track for the pin-on-disk measurements at 25 and 600 °C, for samples V_2O_5-0 and V_2O_5-75, respectively. The spectra clearly indicated that the V_2O_5 structure remained unaltered after the wear test at 25°C, and only minor modifications in the spectra were introduced after the testing at 600°C. These modifications are more pronounced for the V_2O_5-0 sample that shows the disorder-associated peaks around 800-1000 cm^{-1} described in section 3.3. Similar spectra were obtained for the other samples, confirming that the coatings were not completely penetrated to substrate during the wear tests, as was previously detected during the depth profile measurements.

4 Discussion

The objective of this study was to evaluate the effect of Si additions on the structure, morphology and tribo-mechanical properties of vanadium pentoxide coatings. For this

purpose a series of V_2O_5:Si coatings were produced by co-sputtering of independent V and Si targets.

Prior to discussing the implications of our findings, it is worth recapitulating certain key points. The structural analysis (Figs. 1 and 3) confirmed the formation of α-V_2O_5 phase, in good agreement with previous studies reporting formation of orthorhombic phase of α-V_2O_5 at 350 °C [11, 17]. The addition of Si into the α-V_2O_5 induced significant changes in both the structure and morphology of the coatings. The samples deposited at PASi ≤ 50 W presented a mixed (200) + (001) crystalline orientation of the orthorhombic α-V_2O_5 phase but changed to a preferred (001) orientation for larger powers applied to the Si target. This texture changed was also evident in the surface morphology of the V_2O_5 crystals as observed by SEM. Similar variations in the preferred orientation have been reported for metal nitrides, when Si is incorporated [29, 30, 50-52]. It was also shown that the PASi and/or the Si additions induced a shrinking in the crystalline domains whose size reduced progressively from 38 to 6 nm by increasing the Si content to 7.1 at. % (150 W). The grain size could not be calculated for V_2O_5-200 due to the XRD-amorphous structure of this coating. In parallel, a significant increment in the coating's hardness from 3.6 to 16.1 GPa was obtained, which could be explained in terms of the traditional Hall-Petch effect (PASi ≤ 75W). Further additions of Si led to a decrement in the hardness, possible due to the anomalous Hall-Petch effect, as has been reported for other materials [45, 46, 53], or because the loss of the long-range ordering of the V_2O_5 structure.

These first results demonstrated that it is possible to increase the hardness of the oxide coatings by a doping controlled nanostructure sizing. Moreover, the addition of Si into the V_2O_5 coatings did not affect the temperature dependence of the CoF and the values obtained are comparable to those reported in the literature [1, 3, 20]. The V_2O_5-PASi samples (PASi ≤

75W) showed a decreased in the CoF as the temperature was increased and the CoF values obtained are similar to those reported by Gulbinski et al. [20]: about 0.8 at 100 °C and 0.35 at 600 °C. However, the CoF are higher than those obtained by Fateh et al. [18] (0.55 at RT and 0.15 at 600 °C). Samples oriented along the (200) basal planes are expected to present the lowest CoF due to the lamellar structure of the orthorhombic V_2O_5 phase, which might explain the lower CoF observed by Fateh et al. [17] since their samples presented a preferential (200) orientation. Gulbinsky et al. [20] obtained randomly oriented samples and our samples showed a (200) + (001) mixture or a (001) single orientation, but not a purely (200) texture.

From a material's point of view, the effect of the addition of Si into the tribological properties of the V_2O_5 coatings could be analyzed based on the empirical models proposed to correlate the chemical bonding properties of the oxides to the lubricity. However, it needs to be mentioned that such models are not considering that the tribological tests are affected by all the interfaces involved including the ball material, transfer layers and the contribution from the environment (humidity for example).

Erdemir [1] proposed a crystal-chemical approach which empirically relates the CoF to the ionic potential (IP). The IP is easily calculated as the ratio between the charge-state of the cation to its radius; the IP is an estimation of the degree of screening of the cation by the surrounding anions. The crystal-chemical approach [1] predicts that the higher the IP, the lower the CoF at elevated temperatures. The greater the screening of cations in an oxide by the surrounding anions (larger IPs) will allow them to shear more easily leading to the low CoF. On the other hand, Prakash and Celis [3] made a different analysis to explain the relation between the CoF of different oxides and their homologous temperature based on the Yamashita-Kurosawa interaction (YK) parameter [54], instead of the IP. Derived from their

analysis, the authors concluded that the CoF for specific materials decreases as their YK parameter decreases and it was shown valid for three different T/T_m ranges. The YK parameter was estimated by Dimitrov et al. [55] for different oxides and correlated to other properties of the oxides, such as the polarizability, the optical basicity and the O1s binding energy. The conclusion was that the YK parameter represents better the polarizability of both the cations and anions, as well as the ionicity of the bond, so it is more general to classify the oxides than the IP.

Despite some conceptual discrepancies between the two models, both agree that based on either its IP or YK parameter, V_2O_5 can be considered a lubricious oxide. Similarly, both models analyze the extent of adhesive interactions between two or more oxides at a sliding interface; however, their prediction about the effect of mixing SiO_2 to V_2O_5 is slightly different, as discussed below.

Our aim was to enhance the hardness of V_2O_5 or reduced wear by adding Si during the deposition, an effect that was demonstrated in Figure 5 and explained as a consequence of the grain refinement induced by the Si addition. Silicon was chosen based on the previous knowledge about the incorporation of Si into metal nitride coatings, which usually lead to hardness enhancement due to the formation of a covalently bonded SiN_x layer surrounding the metal nitride nanocrystals. In the present study, we expected that Si will bond to oxygen during the reactive deposition forming a SiO_x secondary phase, as was shown by XPS. According to both Erdemir's and Prakash & Celis's models [1, 3], the lubricity of a mixed oxide system will depend on the absolute difference in the IP or the rule of mixture for the YK parameter, respectively. Erdemir [1] proposed that the higher the difference in the IP between the oxides, the higher the lubricity effect. The IP of SiO_2 is 9.8, which is not very different from the 8.4 IP of the V_2O_5 and therefore no significant change of the CoF is

expected from mixing these two oxides, but nothing can be said about the proportion between them. However, from the YK parameter approach, a numerical estimation of the mixture effect can be done since the YK parameter of the composite material is calculated using the rule of mixtures. Therefore, taking the YK values for V_2O_5 (0.057) and SiO_2 (0.216) [55], the YK value of the composite material will continuously increase from 0.057 to 0.216 as the Si content is increased, and in consequence the CoF is also expected to increase. However, the degree of change in the CoF cannot be predicted from this correlation. Experimentally, the results shown in Figure 7 indicated that at high temperatures (≥ 300 °C) even minor variations in the YK parameter of the composite material led to a significant increase in the CoF, as observed for the V_2O_5-75 and V_2O_5-50 samples, whose CoF changed from 0.36 to 0.47 at 600 °C.

The results indicated that the tribological properties of the intermixed phase are very sensitive to the degree of ionicity of the chemical bonds involved. Therefore, the rule mixture of the YK parameter gives us some insights for designing mixed oxide phases with tailored tribological properties, but its validity into other sliding conditions requires further evaluation.

5 Conclusions

In this study, silicon was added to pentoxide vanadium coatings with the aim of increasing the mechanical properties of the coatings. The results show a significant increment in hardness value of α-V_2O_5 from 3.6 to 16.1 GPa by addition of 1.1 at. % Si (PASi=75) due to the observed reduction in grain sizes from 38 to 11 nm. Segregation of neither Si-based particles nor VSi_x based phases was observed in the V_2O_5-PASi (PASi= 0-200 W) samples according to the microstructural analyzes of the coatings by XRD, SEM and Raman. The increment in the hardness values is associated to the reduction of grain sizes in compliance

with the Hall-Petch effect. The results suggest that at low Si concentrations, the SiO_x phase is amorphous and allocated as a thin layer of amorphous SiO_x at grain boundaries, which prevents the growth of the α-V_2O_5 crystalline domains. However, as more Si is incorporated (PASi>75 W), the α-V_2O_5 grain sizes were reduced below 10 nm while the SiO_x amorphous layer probably grow in thickness, leading to a drastic decrease in the hardness, which need to be explains in terms of the establishment of a new deformation mechanism. The tribological results indicated that the crystalline coatings presented a reduction in the CoF as the temperature was increased from 0.9 at RT to about 0.35 - 0.4 at 600 °C, but not significant changes in the CoF values as far as the Si content remains low. Interestingly, the wear rate was also reduced as a function of the temperature, while for the harder sample (V_2O_5-75), the wear rate was lower and independent of the temperature.

6 Acknowledgments

This work was supported by DGAPA-PAPIIT (100116); PASPA-DGAPA, The Royal Society (Newton Advanced Fellowship NA160021). RM-R acknowledged CONACYT for the PhD scholarship. We are also thankful to the academic technicians of the UNAM: Adriana Tejeda, Omar Novelo, Josué Romero, Carlos Ramos and Hermilo Zarco.

7 References

[1] A. Erdemir, Surf Coat Tech, 200 (2005) 1792-1796.
[2] S.M. Aouadi, H. Gao, A. Martini, T.W. Scharf, C. Muratore, Surface and Coatings Technology, 257 (2014) 266-277.
[3] B. Prakash, J.P. Celis, Tribology Letters, 27 (2007) 105-112.
[4] M.N. Gardos, Tribology Transactions, 31 (1988) 427-436.
[5] M.N. Gardos, H.-S. Hong, W.O. Winer, Tribology Transactions, 33 (1990) 209-220.
[6] S.M. Aouadi, B. Luster, P. Kohli, C. Muratore, A.A. Voevodin, Surface and Coatings Technology, 204 (2009) 962-968.
[7] A.A. Voevodin, C. Muratore, S.M. Aouadi, Surface and Coatings Technology, 257 (2014) 247-265.
[8] J. Lin, J.J. Moore, B. Mishra, M. Pinkas, W.D. Sproul, Acta Materialia, 58 (2010) 1554-1564.

[9] R. Franz, C. Mitterer, Surface and Coatings Technology, 228 (2013) 1-13.
[10] S. Surnev, M.G. Ramsey, F.P. Netzer, Progress in Surface Science, 73 (2003) 117-165.
[11] S. Beke, Thin Solid Films, 519 (2011) 1761-1771.
[12] C. Julien, J.P. Guesdon, A. Gorenstein, A. Khelfa, I. Ivanov, Applied Surface Science, 90 (1995) 389-391.
[13] N. Greenwood, A. Earnshaw, Chemistry of the Elements 2nd Edition, Butterworth-Heinemann, 1997.
[14] C.V. Ramana, O.M. Hussain, B.S. Naidu, P.J. Reddy, Thin Solid Films, 305 (1997) 219-226.
[15] N. Fateh, G.A. Fontalvo, G. Gassner, C. Mitterer, Tribology Letters, 28 (2007) 1-7.
[16] W.M. Rainforth, Z. Zhou, in: Journal of Physics: Conference Series, IOP Publishing, 2006, pp. 89.
[17] N. Fateh, G. Fontalvo, C. Mitterer, Journal of Physics D: Applied Physics, 40 (2007) 7716.
[18] N. Fateh, G.A. Fontalvo, C. Mitterer, Tribology Letters, 30 (2008) 21-26.
[19] E. Lugscheider, S. Bärwulf, C. Barimani, Surface and Coatings Technology, 120–121 (1999) 458-464.
[20] W. Gulbiński, T. Suszko, W. Sienicki, B. Warcholiński, Wear, 254 (2003) 129-135.
[21] E. Lugscheider, O. Knotek, K. Bobzin, S. Bärwulf, Surface and Coatings Technology, 133–134 (2000) 362-368.
[22] L. Shizhi, S. Yulong, P. Hongrui, Plasma Chemistry and Plasma Processing, 12 (1992) 287-297.
[23] S. Veprek, A. Niederhofer, K. Moto, T. Bolom, H.D. Mannling, P. Nesladek, G. Dollinger, A. Bergmaier, Surf Coat Tech, 133 (2000) 152-159.
[24] R.F. Zhang, S. Veprek, Phys Rev B, 76 (2007).
[25] P. Karvankova, H.D. Mannling, C. Eggs, S. Veprek, Surf Coat Tech, 146 (2001) 280-285.
[26] D. Bernoulli, U. Muller, M. Schwarzenberger, R. Hauert, R. Spolenak, Thin Solid Films, 548 (2013) 157-161.
[27] A.A. Voevodin, A.L. Yerokhin, V.V. Lyubimov, M.S. Donley, J.S. Zabinski, Surface and Coatings Technology, 86–87, Part 2 (1996) 516-521.
[28] R. Mirabal-Rojas, S. Muhl, S.E. Rodil, E. Camps, M. Lejeune, A. Zeinert, Journal of Vacuum Science & Technology A: Vacuum, Surfaces, and Films, 34 (2016) 041518.
[29] I.-W. Park, D.S. Kang, J.J. Moore, S.C. Kwon, J.J. Rha, K.H. Kim, Surface and Coatings Technology, 201 (2007) 5223-5227.
[30] Y.-C. Lu, H.-W. Chen, C.-C. Chang, C.-Y. Wu, J.-G. Duh, Surface and Coatings Technology, 338 (2018) 69-74.
[31] S.J. Bull, Journal of Physics D: Applied Physics, 38 (2005) R393.
[32] W.C. Oliver, Pharr, G.M, Journal of Material Research, 7 (1992) 1564-1583.
[33] C.V. Ramana, R.J. Smith, O.M. Hussain, C.M. Julien, Journal of Vacuum Science & Technology A: Vacuum, Surfaces, and Films, 22 (2004) 2453-2458.
[34] D.R. Lide, H.V. Kehiaian, CRC Handbook of Thermophysical and Thermochemical Data, CRC Press, 1994.
[35] A. Gies, B. Pecquenard, A. Benayad, H. Martinez, D. Gonbeau, H. Fuess, A. Levasseur, Solid State Ionics, 176 (2005) 1627-1634.
[36] R.T. Rajendra Kumar, B. Karunagaran, S. Venkatachalam, D. Mangalaraj, S.K. Narayandass, R. Kesavamoorthy, Materials Letters, 57 (2003) 3820-3825.
[37] M. Benmoussa, E. Ibnouelghazi, A. Bennouna, E.L. Ameziane, Thin Solid Films, 265 (1995) 22-28.

[38] K. Sieradzka, D. Wojcieszak, D. Kaczmarek, J. Domaradzki, G. Kiriakidis, E. Aperathitis, V. Kambilafka, F. Placido, S.G. Song, Opt Appl, 41 (2011) 463-469.
[39] C. Piccirillo, R. Binions, I.P. Parkin, Chem Vapor Depos, 13 (2007) 145-151.
[40] L. Abello, E. Husson, Y. Repelin, G. Lucazeau, Spectrochimica Acta Part A: Molecular Spectroscopy, 39 (1983) 641-651.
[41] S.-H. Lee, H.M. Cheong, M.J. Seong, P. Liu, C.E. Tracy, A. Mascarenhas, J.R. Pitts, S.K. Deb, Solid State Ionics, 165 (2003) 111-116.
[42] N. Fateh, G.A. Fontalvo, C. Mitterer, J Phys D Appl Phys, 40 (2007) 7716-7719.
[43] E.O. Hall, P Phys Soc Lond B, 64 (1951) 742-&.
[44] N.J. Petch, J Iron Steel I, 174 (1953) 25-28.
[45] H. Ryou, J.W. Drazin, K.J. Wahl, S.B. Qadri, E.P. Gorzkowski, B.N. Feigelson, J.A. Wollmershauser, ACS Nano, (2018).
[46] C.S. Pande, K.P. Cooper, Progress in Materials Science, 54 (2009) 689-706.
[47] X. Zhang, H. Wang, R.O. Scattergood, J. Narayan, C.C. Koch, Acta Materialia, 50 (2002) 3995-4004.
[48] J. Schiøtz, F.D. Di Tolla, K.W. Jacobsen, Nature, 391 (1998) 561.
[49] W.M. Rainforth, Journal of Materials Science, 39 (2004) 16.
[50] E. Martinez, R. Sanjinés, O. Banakh, F. Lévy, Thin Solid Films, 447–448 (2004) 332-336.
[51] D. Oezer, G. Ramirez, S.E. Rodil, R. Sanjines, J Appl Phys, 112 (2012).
[52] G. Ramirez, D. Oezer, M. Rivera, S.E. Rodil, R. Sanjines, Thin Solid Films, 558 (2014) 104-111.
[53] C.E. Carlton, P.J. Ferreira, Acta Materialia, 55 (2007) 3749-3756.
[54] J. Yamashita, T. Kurosawa, Journal of the Physical Society of Japan, 10 (1955) 610-633.
[55] V. Dimitrov, T. Komatsu, Journal of Solid State Chemistry, 163 (2002) 100-112.

Table I. Deposition conditions and main results for the samples deposited on the D2 substrate: Thickness, Si content, V/O composition ratio, crystalline domain size, hardness and modulus of elasticity of all deposited coatings.

Sample	Power (W)	Thickness (nm)**	Si at. %*	V/O*	Crystalline Domain (nm)*	Hardness** (GPa)	Young's Modulus** (GPa)
V_2O_5-0	0	1245 ± 49	-	0.38 ± 0.14	38 ± 2	3.6 ± 0.3	132.4 ± 3.5
V_2O_5-12	12.5	1371 ± 54	-	0.39 ± 0.14	32 ± 2	4.9 ± 0.3	180.4± 4.7
V_2O_5-25	25	1427 ± 43	-	0.37 ± 0.14	22 ± 2	10.4 ± 0.2	200.0 ± 2.3
V_2O_5-50	50	1595 ± 48	0.8± 0.1	0.38 ± 0.14	16 ± 2	13.8 ± 0.2	237.8 ± 4.2
V_2O_5-75	75	1704 ± 51	1.1± 0.1	0.39 ± 0.14	11 ± 2	16.1 ± 0.2	240.9 ± 3.5
V_2O_5-100	100	1897 ± 57	1.3± 0.1	0.38 ± 0.14	8 ± 2	11.0 ± 0.1	205.7 ± 4.3
V_2O_5-150	150	2104 ± 42	7.1± 0.7	0.30 ± 0.14	6 ± 2	4.1 ± 0.2	168.9 ± 4.5
V_2O_5-200	200	2298 ± 46	9.7± 0.9	0.29 ± 0.14	-	2.9 ± 0.2	127.4 ± 2.5

*median ± standard error

**mean ± standard deviation

Figure Captions

Figure 1. SEM micrographs: Backscattering electron images of a) V_2O_5-0, b) V_2O_5-12.5, c) V_2O_5-25, d) V_2O_5-50, e) V_2O_5-75, f) V_2O_5-100, g) V_2O_5-150, and h) V_2O_5-200 coatings.

Figure 2. Si 2p high resolution X-ray photoelectron spectra (a) and composition (b) for the V_2O5:Si coatings as a function of the power applied to the silicon target (PASi).

Figure 3. XRD: Grazing incidence X-ray diffraction patterns ($\alpha = 1°$.) of V_2O_5:Si (PASi: 0-200 W) deposited coatings. The patterns were normalized to their corresponding maximum peak, but large differences in the peak intensities were obtained (Fig. S3) .The pattern of the V_2O_5 (ICDD-00-041-1426) reference data is shown in blue lines.

Figure 4. Raman spectra of all coatings: the lines correspond to the vibrational bands of the α-V_2O_5 phase. The spectra looks alike for the most crystalline samples (PASI < 100 W) with larger intensities while some new weak bands (above 800 cm^{-1}) are observed for the samples deposited at larger PASi.

Figure 5. Nanoindentation: Hardness and elastic modulus variation of the coatings deposited on the D2 steel substrates. The red symbols (online version) indicated samples (12.5 and 25 PASi) where the Si content could not be measured.

Figure 6. Hall-Petch plot: Hardness versus the inverse of the crystalline domain size.

Figure 7. Pin on disk: Coefficient of friction measured at three different temperatures (25, 300 and 600 °C) for the V_2O_5:Si samples as a function of the homologous temperature.

Figure 8. Wear: Wear rate of V_2O_5- X samples (X=0, 25, 50, and 75) and representative Raman spectra outside and inside of the wear scar for the V_2O_5-0 sample (b) and the V_2O_5-75 sample (c).

Table I

Table I. Deposition conditions and main results for the samples deposited on the D2 substrate: Thickness, Si content, V/O composition ratio, crystalline domain size, hardness and modulus of elasticity of all deposited coatings.

Sample	Power (W)	Thickness (nm)**	Si at. %*	V/O*	Crystalline Domain (nm)*	Hardness** (GPa)	Young's Modulus** (GPa)
V_2O_5-0	0	1245 ± 49	-	0.38 ± 0.14	38 ± 2	3.6 ± 0.3	132.4 ± 3.5
V_2O_5-12	12.5	1371 ± 54	-	0.39 ± 0.14	32 ± 2	4.9 ± 0.3	180.4± 4.7
V_2O_5-25	25	1427 ± 43	-	0.37 ± 0.14	22 ± 2	10.4 ± 0.2	200.0 ± 2.3
V_2O_5-50	50	1595 ± 48	0.8± 0.1	0.38 ± 0.14	16 ± 2	13.8 ± 0.2	237.8 ± 4.2
V_2O_5-75	75	1704 ± 51	1.1± 0.1	0.39 ± 0.14	11 ± 2	16.1 ± 0.2	240.9 ± 3.5
V_2O_5-100	100	1897 ± 57	1.3± 0.1	0.38 ± 0.14	8 ± 2	11.0 ± 0.1	205.7 ± 4.3
V_2O_5-150	150	2104 ± 42	7.1± 0.7	0.30 ± 0.14	6 ± 2	4.1 ± 0.2	168.9 ± 4.5
V_2O_5-200	200	2298 ± 46	9.7± 0.9	0.29 ± 0.14	-	2.9 ± 0.2	127.4 ± 2.5

*median ± standard error

**mean ± standard deviation

Figure 1

Click here to download Figure: Figure 1.eps

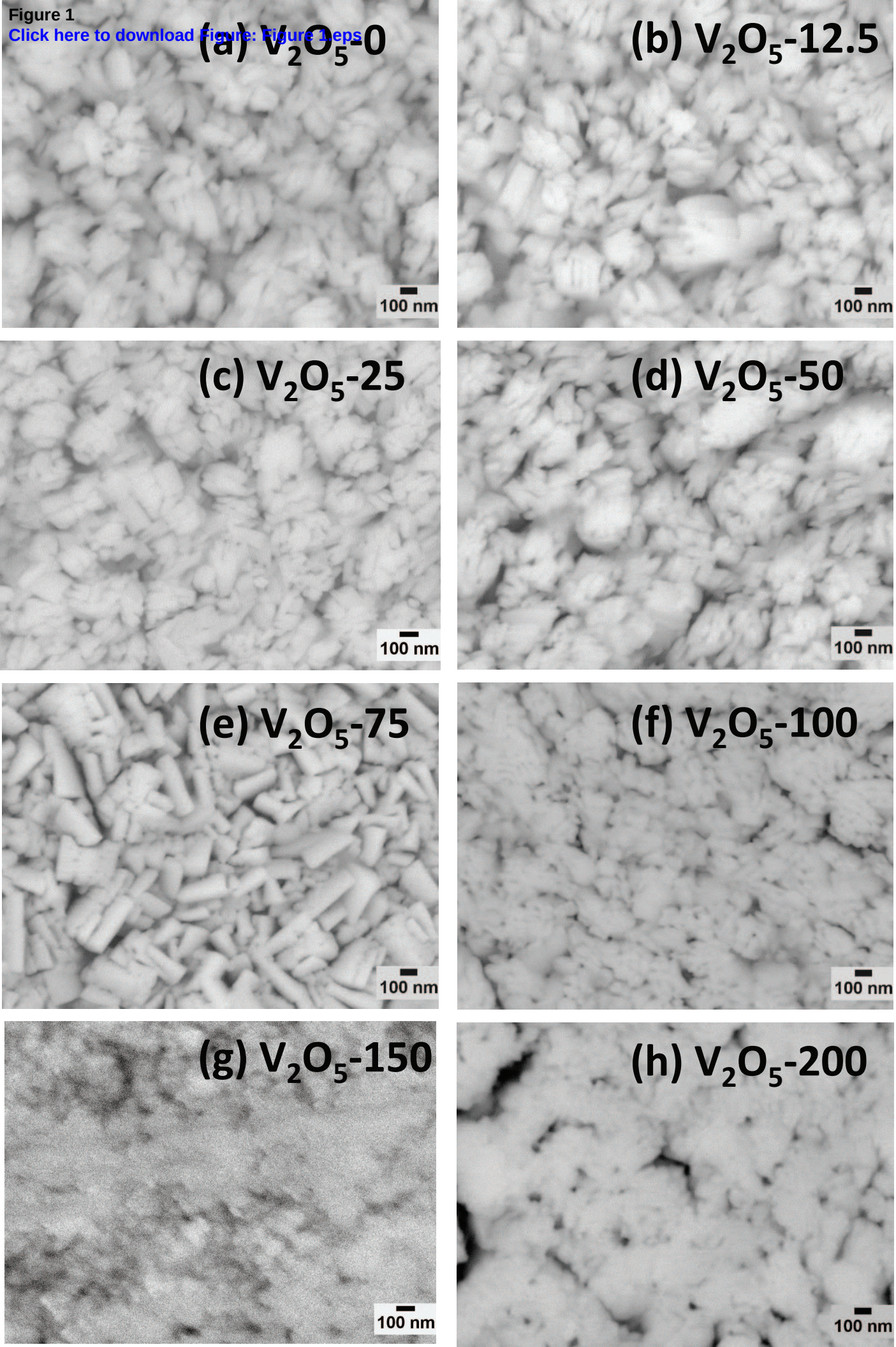

Figure 2a
Click here to download Figure: Figure 2a.eps

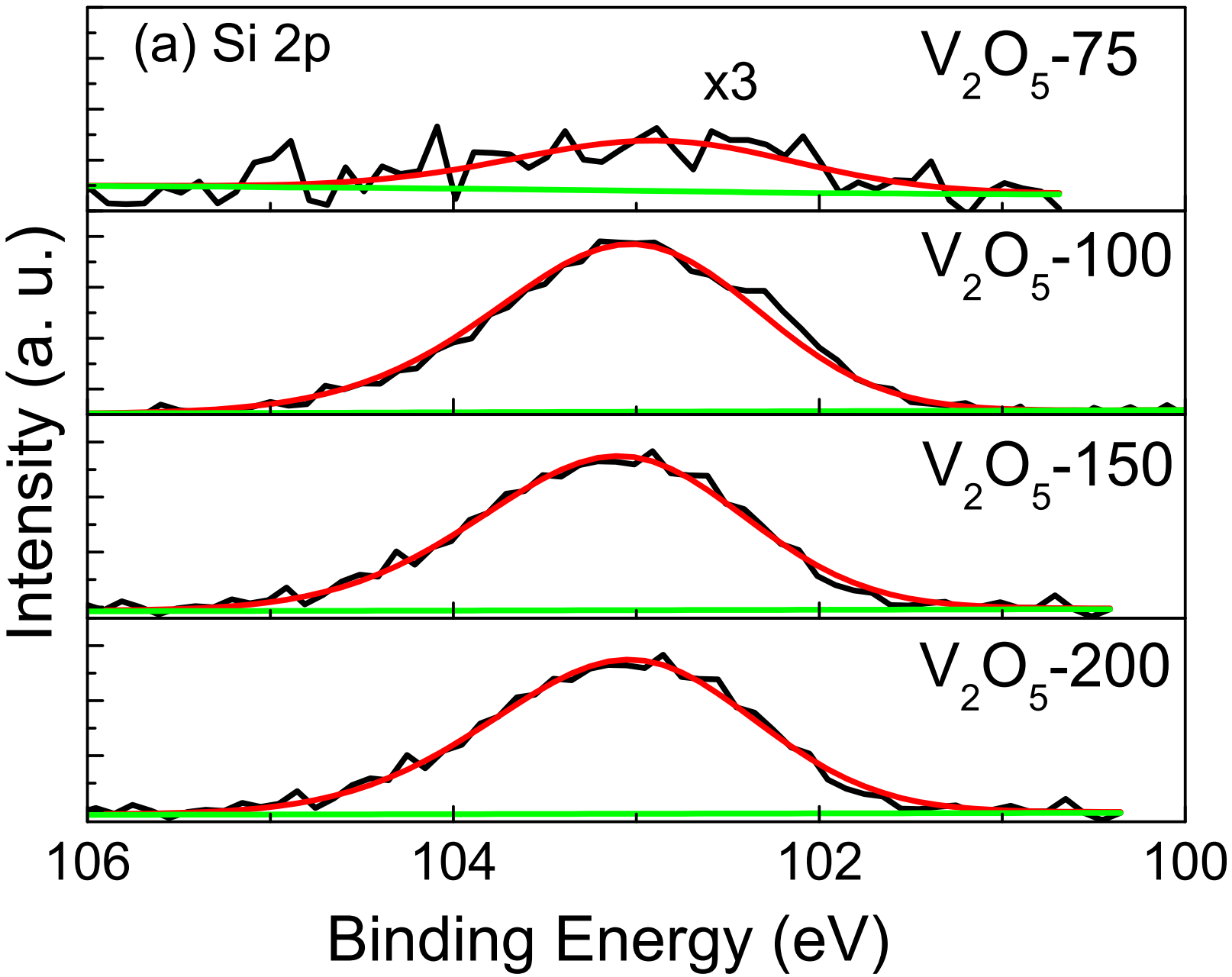

Figure 2b
Click here to download Figure: Figure 2b.eps

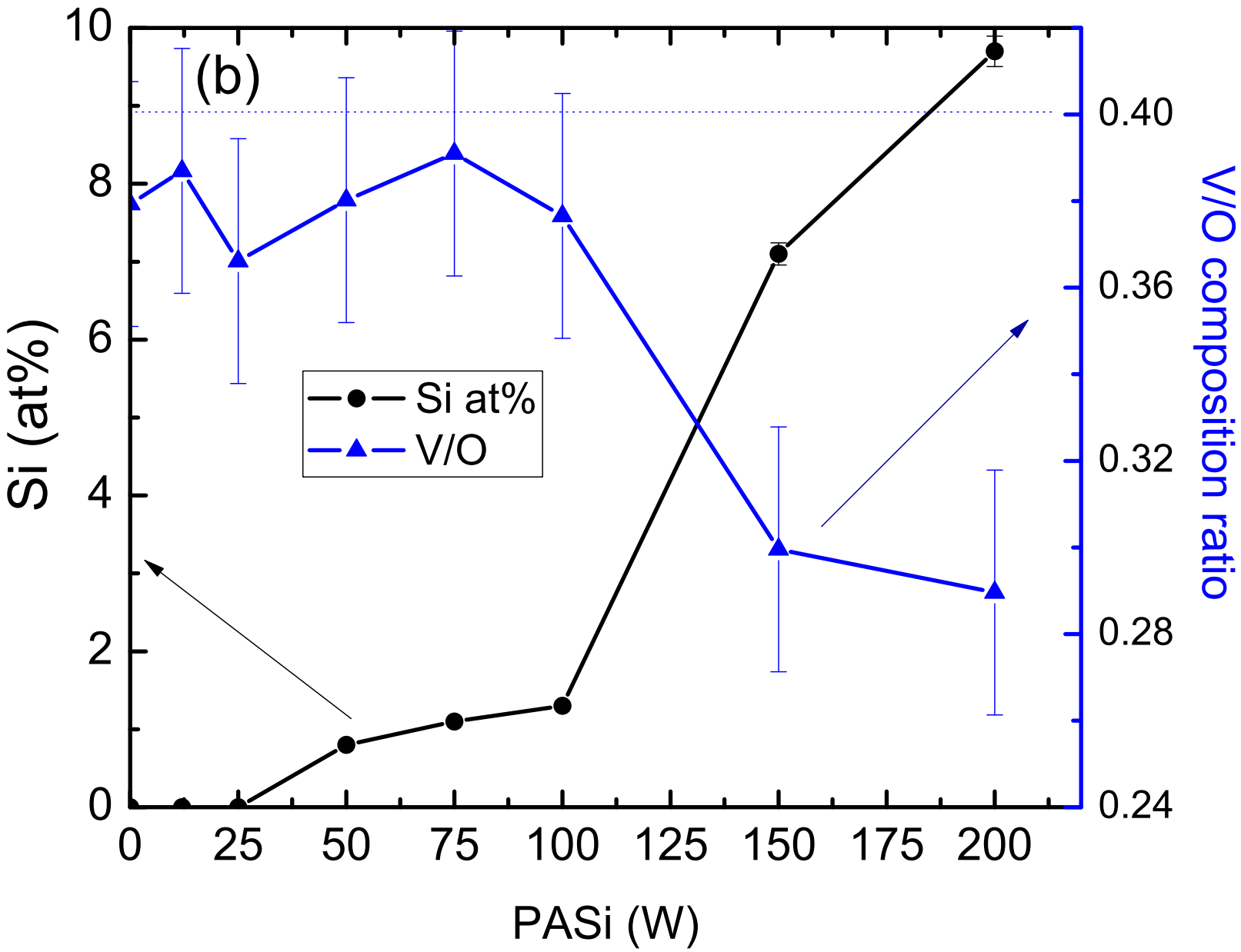

Figure 3

Click here to download Figure: Figure 3.eps

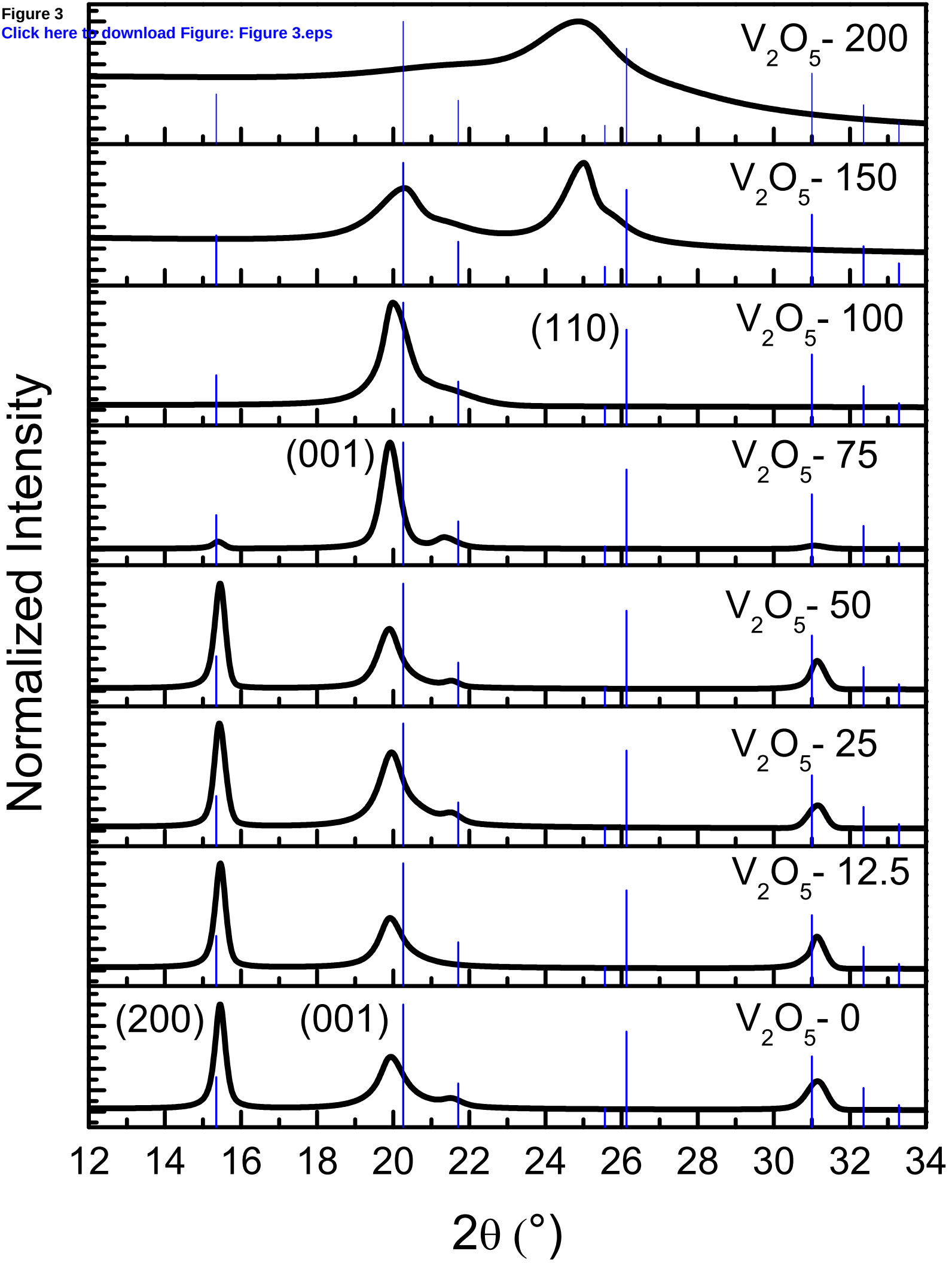

Figure 4

Click here to download Figure: Figure 4.eps

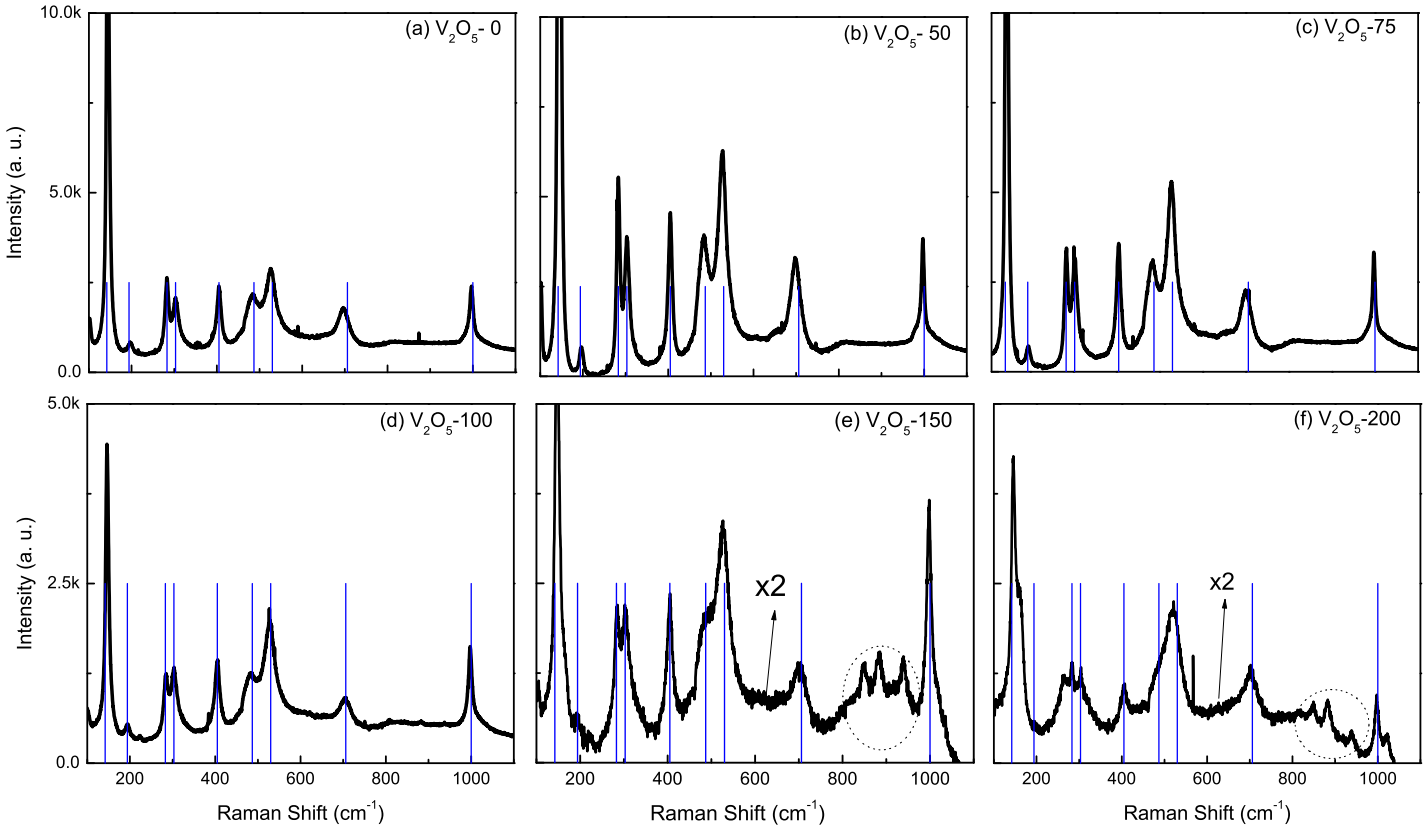

Figure 5
Click here to download Figure: Figure 5.eps

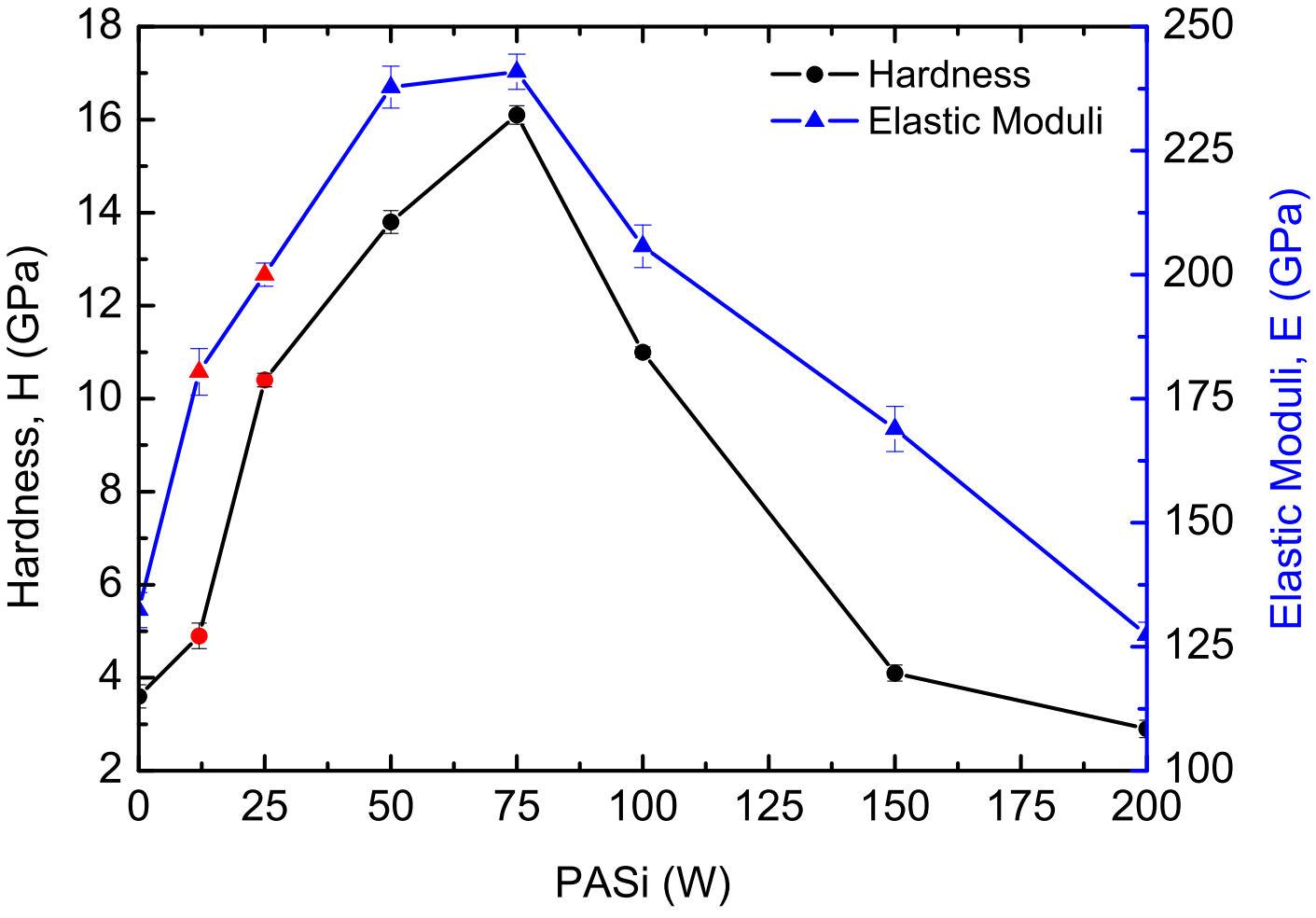

Figure 6
Click here to download Figure: Figure 6.eps

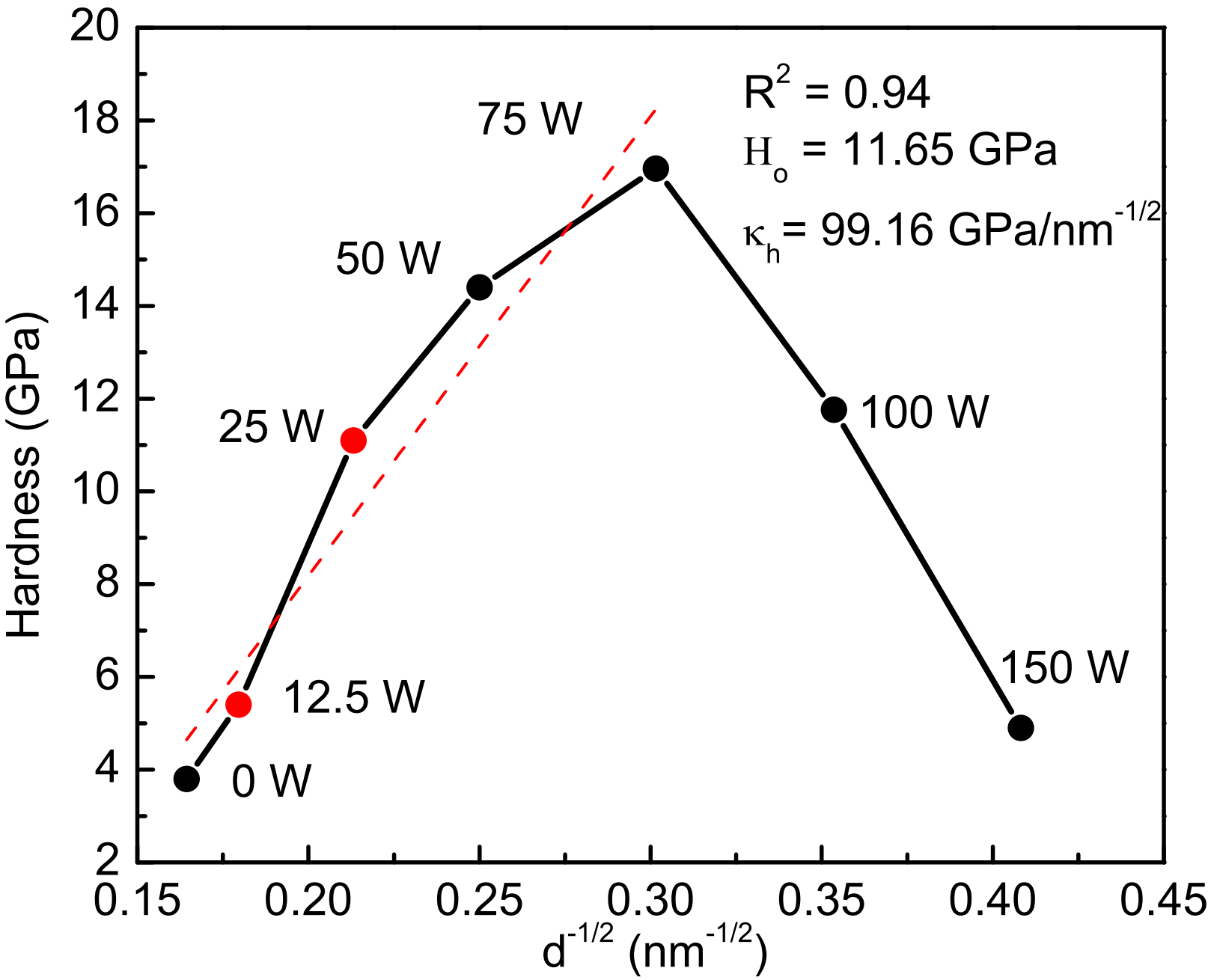

Figure 7
Click here to download Figure: Figure 7.eps

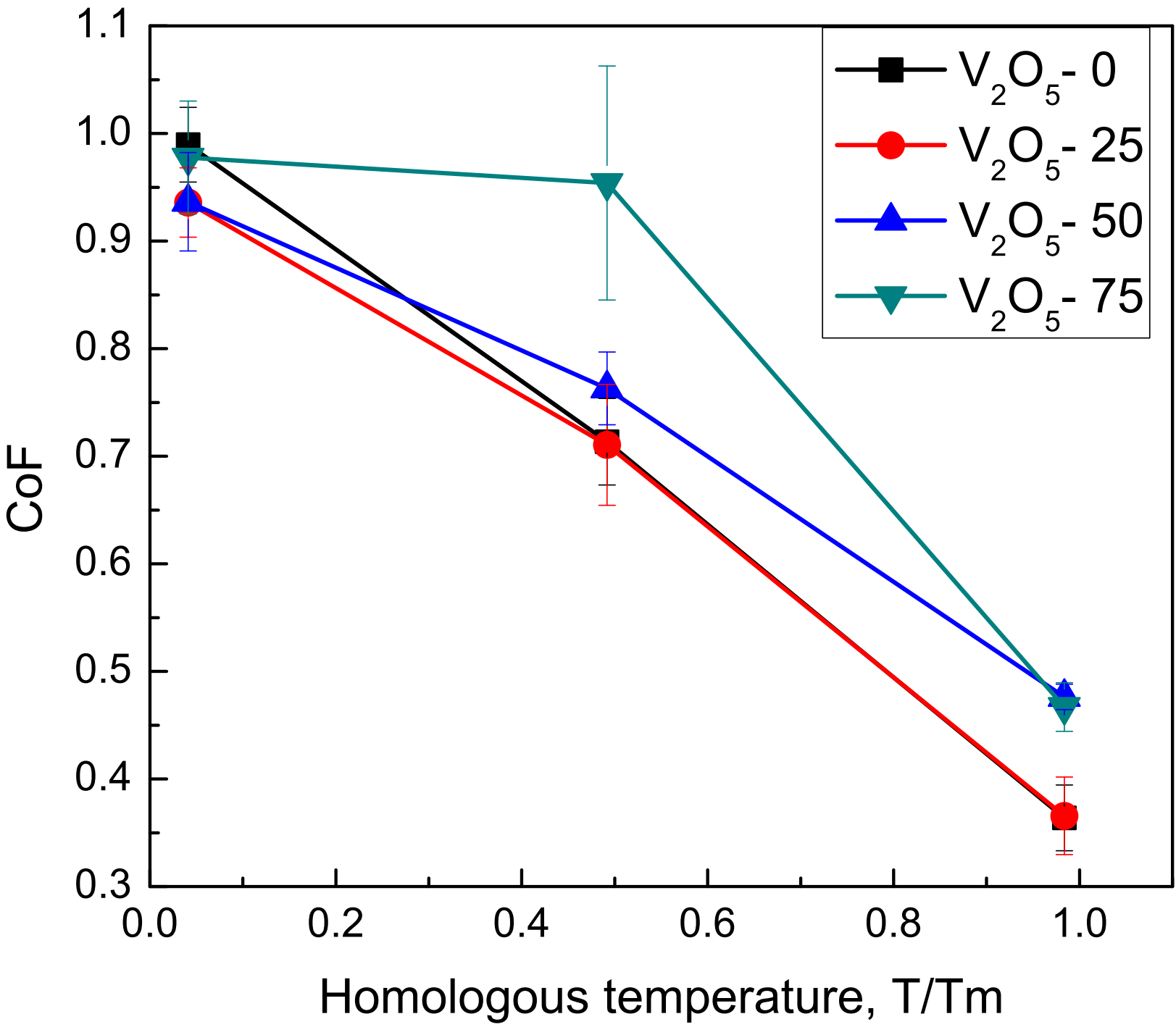

Figure 8a
Click here to download Figure: Figure 8a.eps

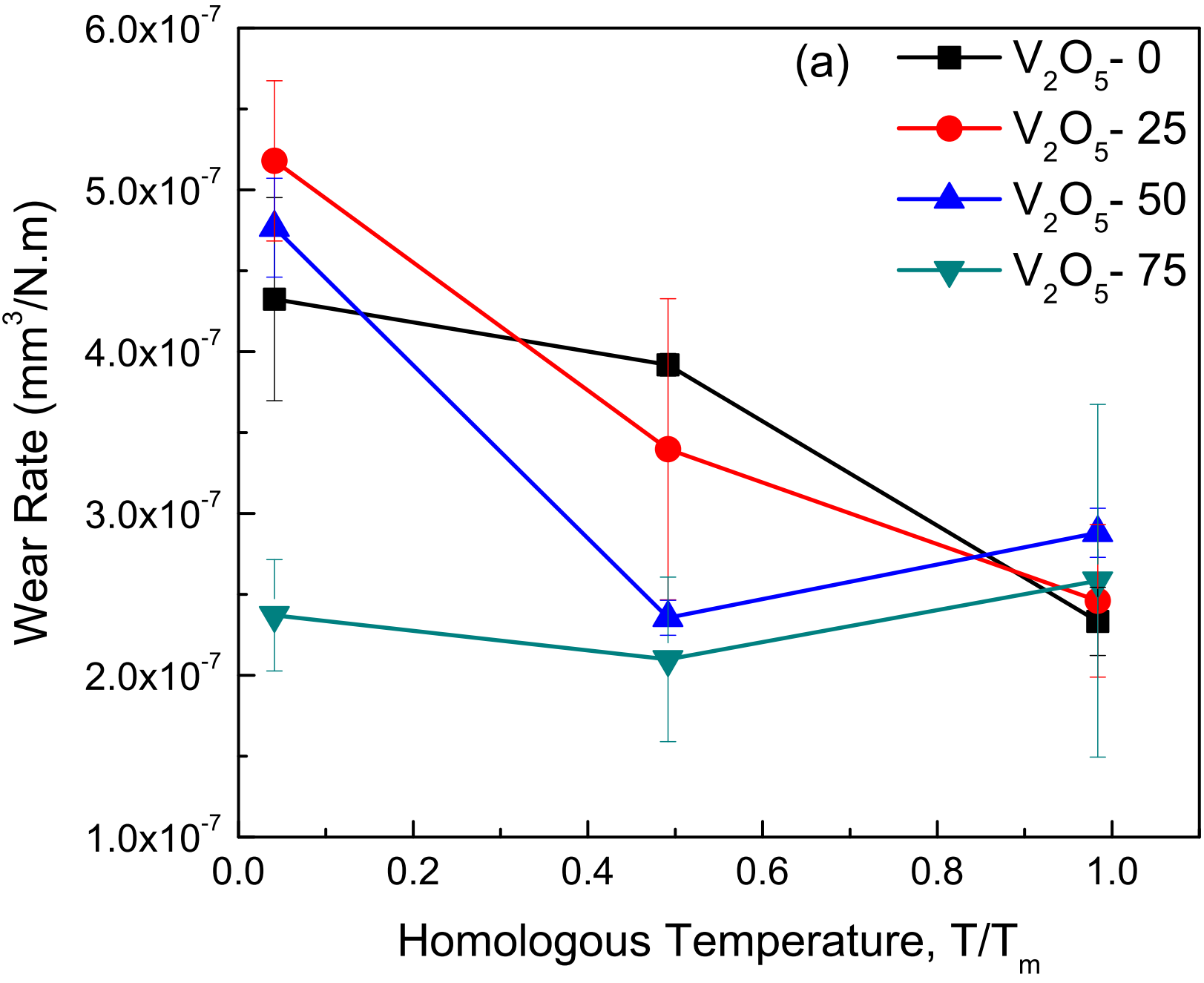

Figure 8b
Click here to download Figure: Figure 8b.eps

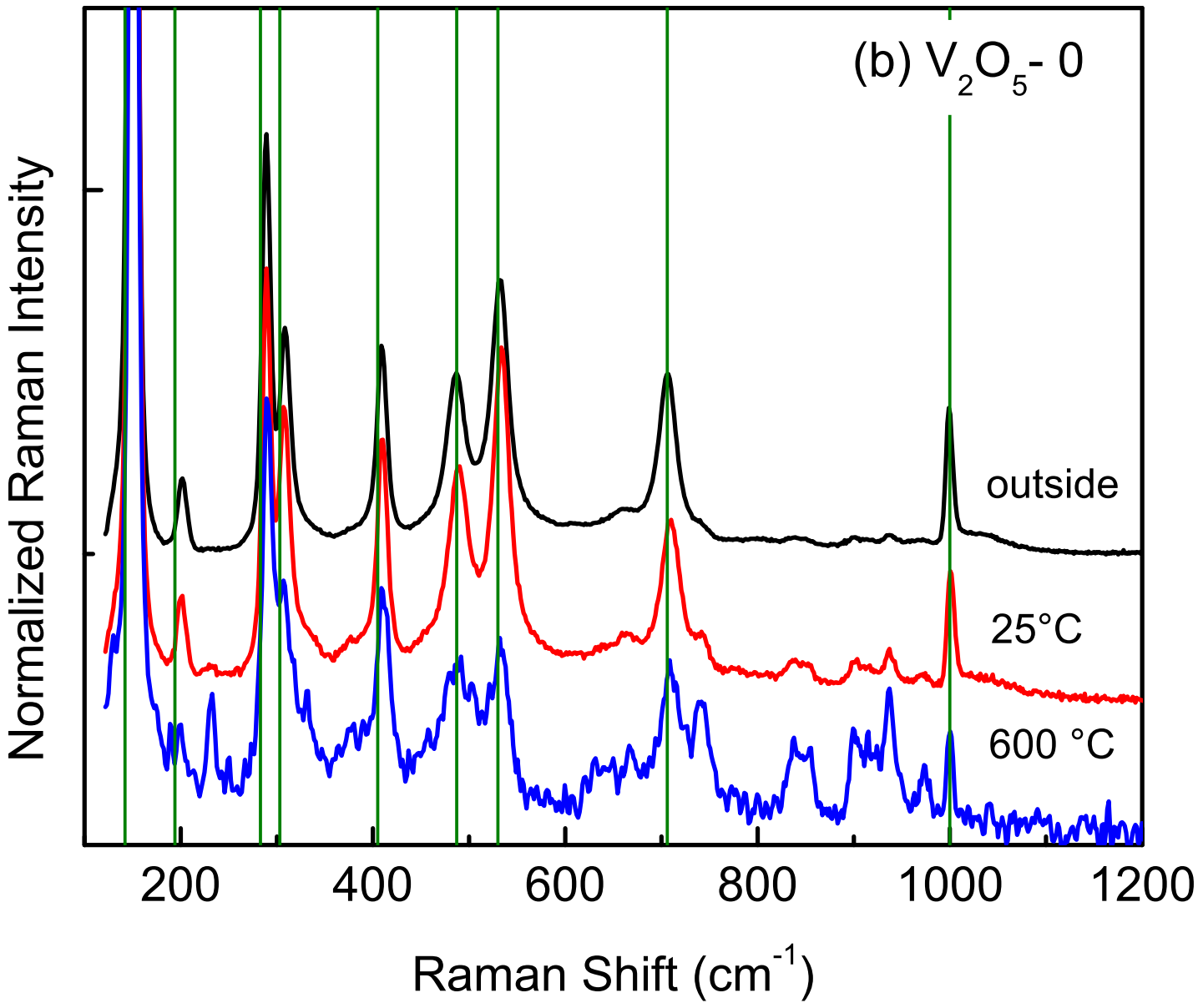

Figure 8c
Click here to download Figure: Figure 8c.eps

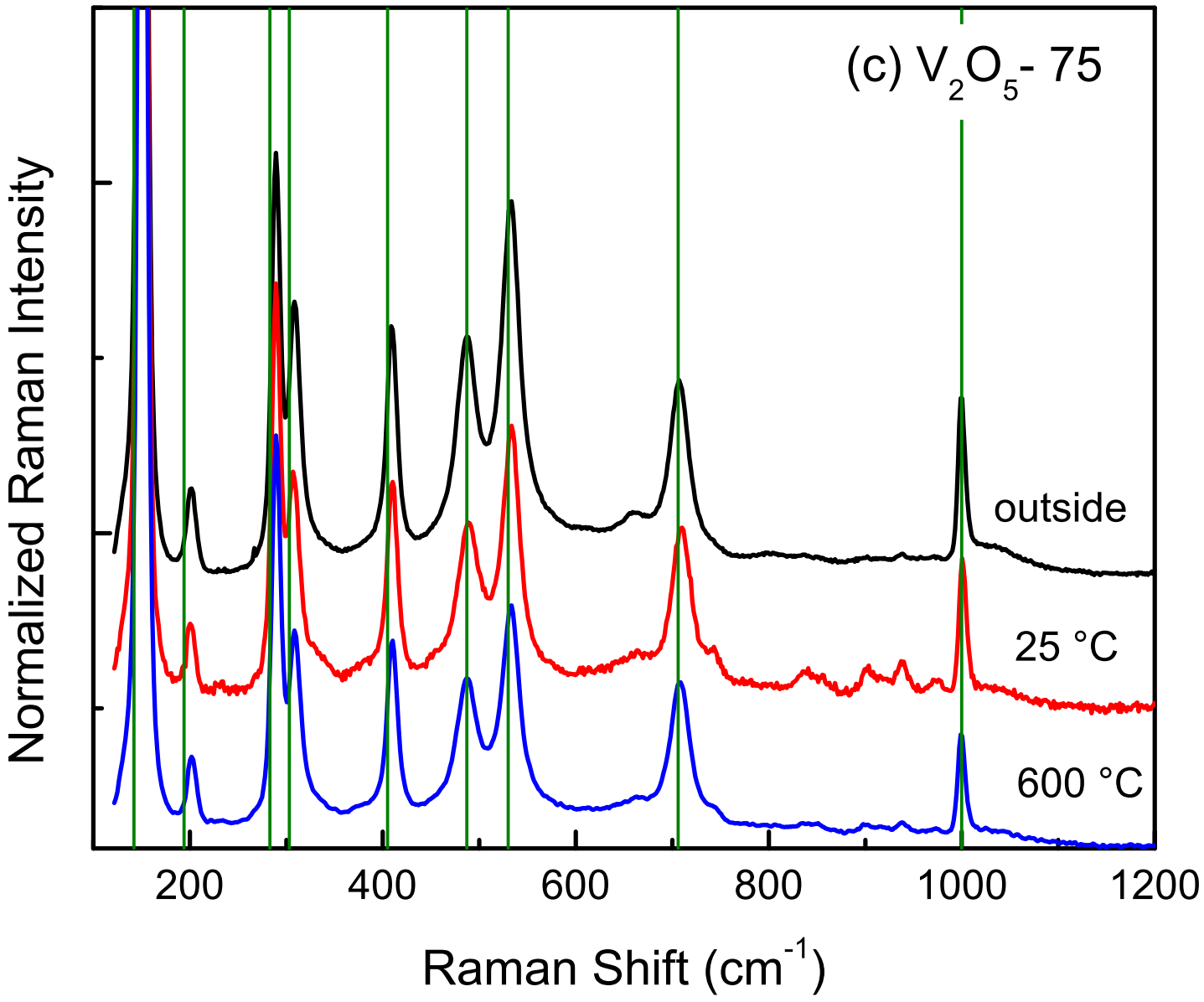

Graphical Abstract